

Tim-3/galectin-9 pathway and mMDSC control primary and secondary resistances to PD-1 blockade in lung cancer patients

Emeric Limagne^{a*}, Corentin Richard^{a,b*}, Marion Thibaudin^a, Jean-David Fumet^{a,c}, Caroline Truntzer^a, Aurélie Lagrange^c, Laure Favier^c, Bruno Coudert^c, and François Ghiringhelli^{a,b,c,d,e}

^aPlatform of Transfer in Cancer Biology, Centre Georges-François Leclerc, Dijon, France; ^bUniv. Bourgogne Franche-Comté, Dijon, France; ^cDepartment of Medical Oncology, Centre Georges-François Leclerc, Dijon, France; ^dCentre de Recherche INSERM LNC-UMR1231, Dijon, France; ^eGenetic and Immunology Medical Institute, Dijon, France

ABSTRACT

Nivolumab, a monoclonal antibody targeting PD-1, is currently approved for metastatic non-small cell lung cancer (mNSCLC) treatment after failure of first-line chemotherapy. However, only a quarter of patients benefit from this therapy with objective clinical response. In this context, there is an unmet need for improved understanding of resistance mechanisms. Thus, we studied a prospective cohort of mNSCLC (n = 61) treated in second or third-line with nivolumab. We analyzed various blood myeloid and lymphoid markers by flow cytometry (176 variables) at baseline, and after 15 and 30 days of therapy. By attempting to link the evolution of peripheral lymphoid, myeloid cells and anti-PD-1 response, we observed that accumulation of lymphoid cells and monocytic MDSC (mMDSC) expressing, respectively, Tim-3 and galectin-9 is implicated in resistance to PD-1 blockade both for patients with primary or acquired secondary resistance to anti-PD-1. In vitro, anti-Tim-3 blocking antibody reverses resistance to anti-PD-1 in PBMC from lung cancer patients and high levels of blood mMDSC negatively impact on anti-PD-1 efficacy. Together, these data underline that the galectin-9/Tim-3 pathway and mMDSC are key mechanisms of primary or secondary resistance to anti-PD-1 and could be a new target for immunotherapy drug combinations.

ARTICLE HISTORY

Received 7 July 2018
Revised 5 November 2018
Accepted 6 November 2018

KEYWORDS

Lung cancer; immune checkpoint; nivolumab; anti-PD-1; Tim-3; MDSC

Introduction


Despite recent advances in the molecular classification of non-small cell lung cancer (NSCLC) and the development of targeted therapies, the prognosis for patients with advanced disease remains poor.¹ Baseline therapy mainly relies on platinum-based chemotherapy or therapies targeting Epidermal Growth Factor Receptor (EGFR) mutational status. Despite the effectiveness of these therapies, the prognosis remains poor due to the ineluctable escape of the disease. Monoclonal antibodies (mAb) targeting “immune” checkpoint inhibitors of the immune response revolutionized the treatment of lung cancer.^{2,3} The CheckMate 057 study⁴ was the first to demonstrate that an anti-PD-1 antibody (nivolumab) provided a better survival advantage than chemotherapy in lung adenocarcinomas that had progressed during or after first-line therapy. These data were further confirmed in squamous and non-squamous cell lung carcinoma treatment using another anti-PD-1 mAb, pembrolizumab,⁵ or the anti-PD-L1 mAb atezolizumab.⁶ Nivolumab, pembrolizumab, and atezolizumab are currently approved for the second- or third-line treatment of squamous cell carcinoma and adenocarcinoma. Despite the undeniable efficacy of these therapies, only a quarter of NSCLC patients experiment a clinical benefit with these new therapies.^{4,7} Consequently, there is an unmet

need for improved understanding of resistance mechanisms to PD-1 blockade, with a view to correctly identifying non-responders, and envisaging new drug combinations, based on a solid biological rationale.

Assessment of tumor PD-L1 expression by immunohistochemistry (IHC) is currently used to select patients. Under first-line therapy, expression of PD-L1 in more than 50% of the cancer cells is associated with better efficacy of pembrolizumab in comparison to chemotherapy.⁸ However, this marker is sub-optimal and does not predict the absence of anti-PD-1 efficacy.^{9,10} This difficulty could be explained by the failure to take account of the immune infiltrate profile, the presence of additional checkpoints such as Tim3, TIGIT or Lag3, the presence of immunosuppressive cells, or the presence of oncogenic induction of PD-L1. Recent data underline suggest a possible role of myeloid-derived suppressor cells (MDSC) in cancer-related immunosuppression, which could mediate resistance to therapies. This population of immature myeloid cells can inhibit anti-tumor activities of T and NK cells and stimulate regulatory T cells (Treg), leading to tumor progression.¹¹ To improve the prediction of response, a growing number of studies have tested some tumor histological or genetic markers, but response prediction remains a conundrum. In contrast, few studies have analyzed peripheral blood. Baseline routine blood parameters were associated with pembrolizumab outcome in melanoma

CONTACT François Ghiringhelli  fgghiringhelli@cgfl.fr  Georges-François Leclerc Cancer Center, 1 rue Professeur Marion, Dijon 21000, France

*These authors contributed equally to this work.

 Supplemental data for this article can be accessed on the publisher's website.

© 2019 The Author(s). Published with license by Taylor & Francis Group, LLC

This is an Open Access article distributed under the terms of the Creative Commons Attribution-NonCommercial-NoDerivatives License (<http://creativecommons.org/licenses/by-nc-nd/4.0/>), which permits non-commercial re-use, distribution, and reproduction in any medium, provided the original work is properly cited, and is not altered, transformed, or built upon in any way.

patients, suggesting that peripheral analysis could be an interesting tool for the identification of markers and biological mechanisms involved in immunotherapy resistance.¹² More recently, John Wherry's group demonstrated in melanoma patients treated with pembrolizumab that T cell invigoration to tumor burden ratio is associated with outcome using immune blood cytometric analysis and clinical data.¹³ We hypothesized that serial multiparametric cytometry analysis during therapy could be used to identify common mechanisms of resistance, and consequently, could be used to detect potential markers of response to anti-PD-1 in NSCLC patients. We prospectively analyzed blood immune parameters of NSCLC patients before and during nivolumab treatment, given as a second or third line. Using this strategy, we observed that early accumulation of monocytic myeloid-derived suppressor cells (mMDSC) expressing galectin-9, and lymphoid cells with high Tim-3 expression is associated with both primary and secondary resistance.

Methods

Patient data

This study included consecutive stage IIIB and IV advanced NSCLC patients, treated at the Georges Francois Leclerc Center with nivolumab anti-PD-1 monotherapy in the second or third line of therapy after approval of nivolumab usage by the French health authorities. First or second line consisted of platinum-based chemotherapy with or without targeted therapy. Patients received nivolumab until progression or unacceptable toxicity. Written informed consent was obtained from all patients before enrollment. The hospital institutional review board approved the study in accordance with the principles of Good Clinical Practice, the Declaration of Helsinki, and other applicable local regulations. This study was declared as a sub-study of an ongoing project registered with ClinicalTrials.gov under the identifier NCT02281214.

Clinical data collection

Included patients received nivolumab at the recommended dose (3 mg/kg q2 weeks). The following data were collected from each patient's medical records: age, sex, smoking status, *EGFR* and *KRAS* mutational status, ECOG performance status at the time of nivolumab initiation, nature of first-line platinum-based doublet, number of treatment lines prior to nivolumab initiation, date of nivolumab initiation, best RECIST 1.1 response to nivolumab, date of progression during or after nivolumab, and death from any cause or last follow-up. The database was opened on 1 May 2015 and closed on 1 February 2017. Two physicians (JDF, AL) reviewed all CT-scans to validate response to nivolumab.

Whole blood of NSCLC patients was sampled before (D0) and after chemotherapy (D15, D30, and D60) on heparinized tubes for leucocyte phenotyping. All analyses were performed within 6 h after sampling. Review of pathology reports confirmed the diagnosis. Information regarding clinical, pathologic, and biological characters of patients and healthy volunteers are presented in Table 1. All data were collected

Table 1. Summary of clinical characteristics of the mNSCLC cohort. Gender, age, smoking status, WHO performance status, tumor histology, and tumor stage are detailed.

Variables		Number (%)
Gender	Female	14 (23)
	Male	47 (77)
Age-yr	median (range)	66 (45–85)
	mean (sd)	66.9 (9.2)
Smoker	No	6 (10)
	yes	55 (90)
WHO performance status	0	26 (43)
	1–2	35 (57)
Tumor histology	Nonsquamous-cell	36 (59)
	Squamous-cell	24 (39)
	Other	1 (2)
Tumor stage	IIIB	8 (13)
	IV	53 (87)
First line doublet	Gemcitabine	16 (26)
	Taxane	16 (26)
	Pemetrexed	26 (44)
	Other	3 (4)
Type of platin	Carboplatin	29 (48)
	Cisplatin	29 (48)
	Other	3 (4)

prospectively, but analyses were performed retrospectively without predetermined hypotheses.

Immunomonitoring

Flow cytometry

Antibodies and cytometry procedure

For T helper identification, anti-CD4-VioGreen (VIT4), anti-CD45RA-APC-Vio770 (T6D11), anti-CD25-APC (3G10), anti-CCR6-PE (REA190), anti-CXCR3-PE-Vio700 (REA232) and anti-Tim-3-FITC (F38-3E2) were purchased from Miltenyi Biotec. Anti-CRTH2-Brilliant Violet 421 (BM16) was purchased from BD Biosciences and anti-PD-1-PerCP-eFluor700 (MIH4) was purchased from eBiosciences.

For T CD8⁺ identification, anti-CD8-VioGreen (BW135/80), anti-CD45RA-APC-Vio770 (T6D11), anti-CD44-APC (DB105), anti-CCR7-PE (REA547), anti-CD62L-PE-Vio770 (145/15), anti-CD3-VioBlue (BW264/56), and anti-Tim-3-FITC (F38-3E2) were purchased from Miltenyi Biotec. Anti-PD-1-PerCP-eFluor700 (MIH4) was purchased from eBiosciences.

For Treg and NK identification, anti-CD4-VioGreen (VIT4), anti-CD45RA-APC-Vio770 (T6D11), anti-CD25-APC (3G10), anti-Foxp3-PE (3G3), anti-CD56-PE-Vio770 (AF12-7H3), anti-CD3-VioBlue (BW264/56) and anti-Tim-3-FITC (F38-3E2) were purchased from Miltenyi Biotec. Anti-PD-1-PerCP-eFluor700 (MIH4) was purchased from eBiosciences.

For myeloid subpopulation identification, anti-CD15-VioGreen (VIMC6), anti-CD33-APC-Vio770 (AC104.3E3), anti-CD123-PE (AC145), anti-CD11c-PE-Vio770 (MJ4-27G12), anti-CD3-FITC (BW264/56), anti-CD19-FITC (LT19), anti-CD20-FITC (LT20), anti-CD56-FITC (REA136) and anti-HLA-DR-VioBlue (AC122) were purchased from Miltenyi Biotec. Anti-CD14-PerCP-eFluor700 (61D3) and anti-PD-L1-APC (MIH1) were purchased from eBiosciences.

Leucocyte population identification and numeration

For leucocyte identification by flow cytometry, whole blood removed to heparinized tubes (100 μ L) was stained with

different antibody cocktails for 15 min at room temperature. After surface staining, 2 mL of red blood cell lysis solution (BD Biosciences) was added for 10 min, centrifuged (350 g, 5 min), and then resuspended in flow cytometry buffer (eBioscience). Foxp3 staining was carried out according to the manufacturer's protocol using the fixation/permeabilization solution (eBioscience). All events were acquired on a BD LSR-II cytometer equipped with BD FACSDiva software (BD Biosciences), and data were analyzed using FlowJo software (Tree Star). The gating strategy is described in Supplementary Figures 1–4.

For myeloid cells, gated on CD14⁺ CD15⁺ cells we select monocytes which are positive for HLA-DR and CD33 as monocytic MDSC (mMDSC), CD14⁺ CD15⁺ CD33⁺ HLA-DR⁻ were considered as granulocytic MDSC (gMDSC). CD15⁺ CD14⁻ are considered as granulocytes. For dendritic cells we select CD14⁻ CD15⁻ HLA-DR⁺ cells. Based on CD11c and CD123 labeling CD11c⁺ CD123⁻ are considered as type 1 classical dendritic cell population (DC1), CD11c⁺ CD123^{int} as type 2 classical dendritic cell population (DC2) and CD123⁺ CD11c⁻ as plasmacytoid dendritic cells (pDC).¹⁴

For T cells, subpopulations were classically defined using CD45RA and CCR7 labeling. CD45RA⁺ CCR7⁺ were considered as naïve cells, CD45RA⁺ CCR7⁻ as effector memory RA cells (EMRA), CD45RA^{low} CCR7⁻ as intermediate EMRA, CD45RA⁻ CCR7⁻ as effector memory cells and CD45RA⁻ CCR7⁺ as central memory cells.¹⁵

Helper T subsets were defined using chemokine receptor labeling. CCR6⁺ CXCR3⁻ cells were considered as Th17 cells, CCR6⁺ CXCR3⁺ cells as Th17-Th1 hybrid phenotype and CCR6⁻ CXCR3⁺ as Th1 cells. CCR6⁻ CXCR3⁻ CRTH2⁺ cells were considered as Th2 cells.¹⁶ Cells with CD45RA⁺ labeling were considered as effector cells and called eTh and CD45RA⁻ were considered as memory cells and called mTh. Regulatory T cells (Treg) were characterized upon CD25⁺ and intracellular Foxp3 labeling.

Human NK cells can be divided into two subsets based on their cell-surface density of CD56⁻CD56^{bright} and CD56^{dim}, each with distinct phenotypic properties. The CD56^{dim} NK-cell subset is more naturally cytotoxic and expresses higher levels of CD16 than the CD56^{bright} NK-cell subset. By contrast, the CD56^{bright} subset has the capacity to produce abundant cytokines following activation but has low natural cytotoxicity.¹⁷

In vitro human experiments

PBMC culture

Human PBMCs were first enriched from cancer patient blood using a separation gradient on a lymphocyte separation medium (Eurobio). After isolation, a small part of PBMCs (0.1.10⁶ cells) was stained to quantify by flow cytometry the expression of Tim-3, PD-1 and PD-L1, galectin-9 on CD8 T cells and mMDSC. Surface staining was carried out with the following antibodies for 15 min at room temperature in the dark. For T CD8 analysis, anti-CD8-VioGreen (BW135/80), anti-anti-CD3-VioBlue (BW264/56) and anti-Tim-3-FITC (F38-3E2) were purchased from Miltenyi Biotec. Anti-PD-1-PerCP-eFluor700 (MIH4) was purchased from eBioscience. For myeloid population

analysis, anti-CD33-APC-Vio770 (AC104.3E3), anti-Galectin-9-PE-Vio770 (RG9-35.7), anti-CD3-FITC (BW264/56), anti-CD19-FITC (LT19), anti-CD20-FITC (LT20), anti-CD56-FITC (REA136) and anti-HLA-DR-Violblue (AC122) were purchased from Miltenyi Biotec. Anti-CD14-Krome Orange (RMO52) and anti-PD-L1-APC (PD-L1) were purchased from Beckman Coulter. All events were acquired by a CytoFlex cytometer equipped with CytExpert software (Beckman Coulter), and data were analyzed using CytExpert software.

The rest of the PBMC (0.25.10⁶ cells/well) were stimulated with plate-bound antibodies against CD3 (OKT3, 0.5 µg/mL, BioXcell) with or without anti-PD-1 (Nivolumab, 10 µg/mL) or anti-Tim-3 (Fisher Scientific, F38-2E2, 10 µg/mL) in 96-well plate flat bottom. Cells were classically harvested on day five (unless otherwise specified) for detection of cytokines by ELISA and surface staining analysis.

Measurement of cytokines

After 5 days of culture, cell culture supernatants were assessed by ELISA for human TNFα and IFNγ (BioLegend) according to the manufacturer's protocol.

Statistical methods

Data analysis was performed using the statistical software R (<http://www.R-project.org/>) and representations were made with Prism 7 (GraphPad, San Diego, CA, USA). Progression-free survival (PFS) was defined as the time from the first day of treatment to the first recorded evidence of disease progression by the RECIST criteria, clinical evaluation or death. Survivors were censored after 6 months. Overall survival (OS) was calculated as the time from the date of the nivolumab treatment start to the date of death and censored after 24 months.

Each distribution of absolute counts of subpopulations of cells between patients and healthy volunteers were compared with Wilcoxon rank-sum test and all boxplots were drawn with median, quartiles and Tukey's whiskers. The distributions of proportions of immunosuppressive markers were compared using the test for the comparison of multicomponent distributions and pie charts were drawn based on the recommendation for graphical display, both developed in SPICE software.¹⁸

Univariate Cox proportional hazards models of all clinical and biological variables at baseline and at D15 were built to compute hazard ratios (HRs) with their 95% confidence intervals (CI). Survival curves were estimated using the Kaplan-Meier method and compared using log-rank tests. Median follow-up was calculated using the reverse Kaplan-Meier method or noted NR (Not Reached), as appropriate. The CoxBoost algorithm was used to fit a multivariate model. This algorithm is particularly adapted to the high dimensional setting where there are more variables than observations and fits a Cox proportional hazards model by component-wise likelihood-based boosting. It allows the selection of variables that are the most associated with survival. The model was estimated using the *CoxBoost*¹⁹ R package. A score was then computed for each patient based on the linear predictor

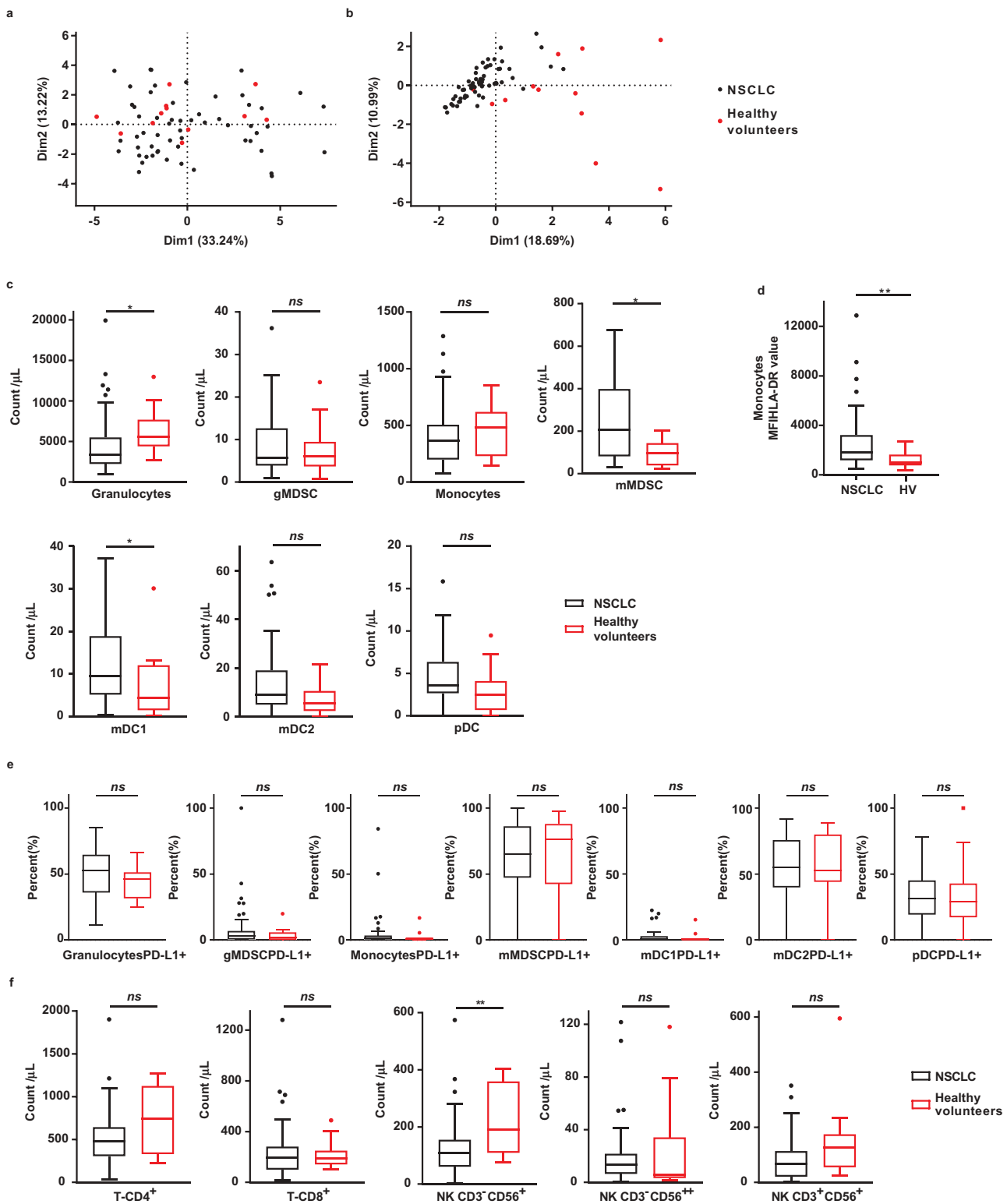


Figure 1. (a-b). Individual factor maps of two principal components analyses including all myeloid parameters (a) and all lymphoid parameters (b). Each individual is represented by a dot; red dots represent healthy volunteers and black dots represent non-small cell lung cancer (NSCLC) patients. Percentages given in brackets correspond to the percent of variance of initial data retained by the axis. (c). Boxplots showing the distribution of the number of cells for different myeloid subpopulations for healthy volunteers (in red) and NSCLC patients (in black). (d). Boxplot showing the distribution of the MFI HLA-DR values for different myeloid cell subpopulations for non-small cell lung cancer patients (NSCLC; in black) and healthy volunteers (HV; in red). (e). Boxplots showing the percent of PD-L1 expressing cells for different myeloid subpopulations for healthy volunteers (in red) and NSCLC patients (in black). (f). Boxplots showing the distribution of the number of cells for different lymphoid subpopulations for healthy volunteers (in red) and NSCLC patients (in black).

*: $p < 0.05$; **: $p < 0.01$; ***: $p < 0.001$; ****: $p < 0.0001$; ns: not significant.

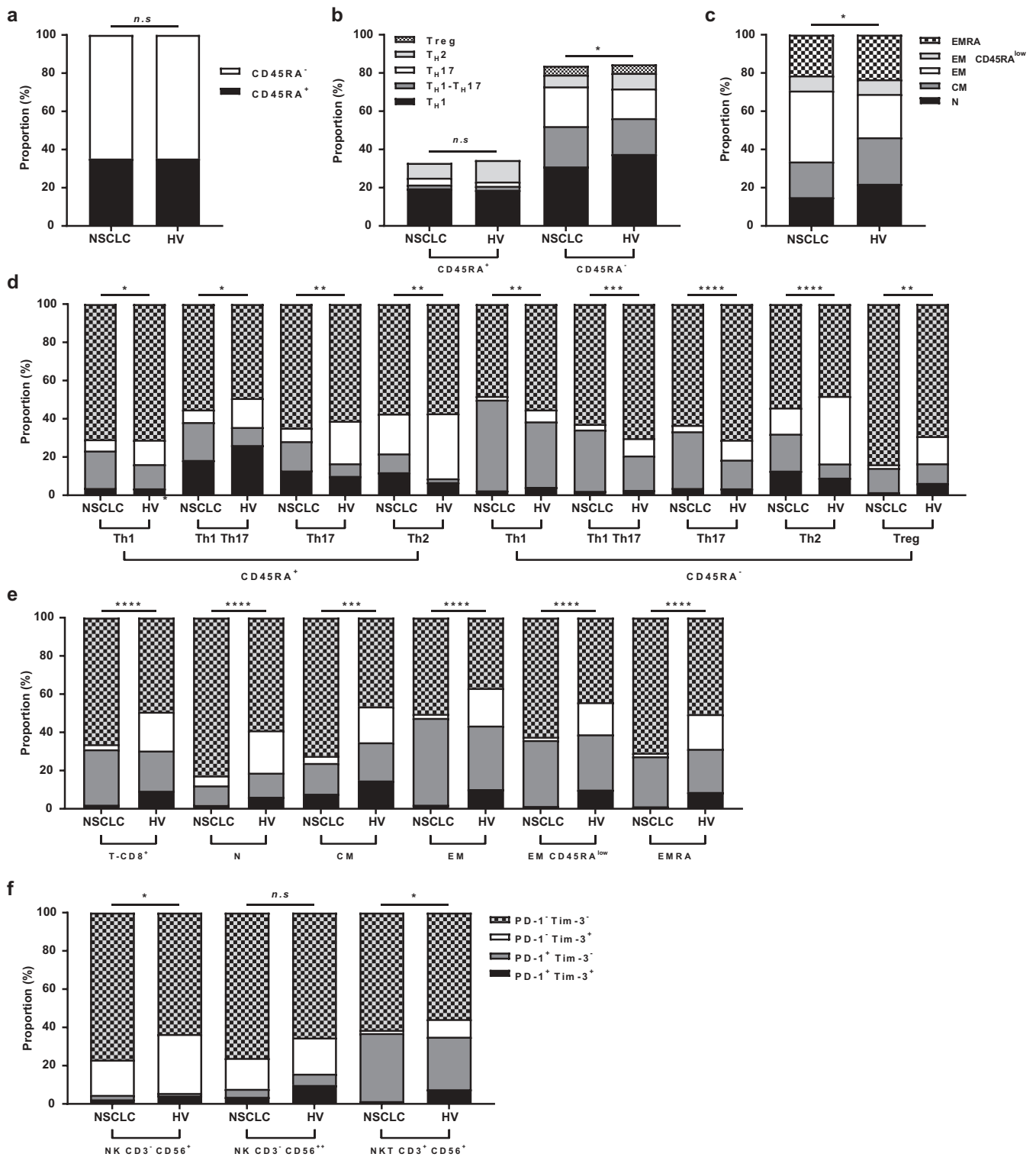


Figure 2. (a). Cumulative bar plots showing the mean proportion of CD45RA⁻ (in white) and CD45RA⁺ (in black) in CD4⁺ T cells for NSCLC patients and HV. (b-c). Cumulative bar plots showing the proportion of different CD4⁺ T subpopulations (Th1, Th2, Th17, Th1-Th17, Treg) in CD45RA⁻ and CD45RA⁺ cells (c) and CD8⁺ T cell subpopulations (Naive, Central Memory, Effector Memory, Effector Memory CD45RA^{low}, Effector Memory RA) for NSCLC patients and HV (d). (d-f). Cumulative bar plots showing the mean proportions of cells expressing both, one or none of the PD-1 and Tim-3 immune checkpoints in CD4⁺ T cells (Th1, Th2, Th17, Th1-Th17, Treg) (e), CD8⁺ T cells (Naive, Central Memory, Effector Memory, Effector Memory CD45RA^{low}, Effector Memory RA) (f) and NK cells (NK CD3⁻ CD56⁺, NK CD3⁻ CD56⁺⁺, NK CD3⁺ CD56⁺) (g) for NSCLC patients and HV.

*: $p < 0.05$; **: $p < 0.01$; ***: $p < 0.001$; ****: $p < 0.0001$; *ns*: not significant.

estimated by the model. A Receiver Operating characteristic (ROC) curve was plotted with the corresponding estimated linear predictor, and the threshold corresponding to the point nearest the upper left corner (best compromise between

sensitivity and specificity) was chosen. The same model was applied to data at D15 without re-estimating the coefficients, and the same threshold was also applied to the resulting linear predictor.

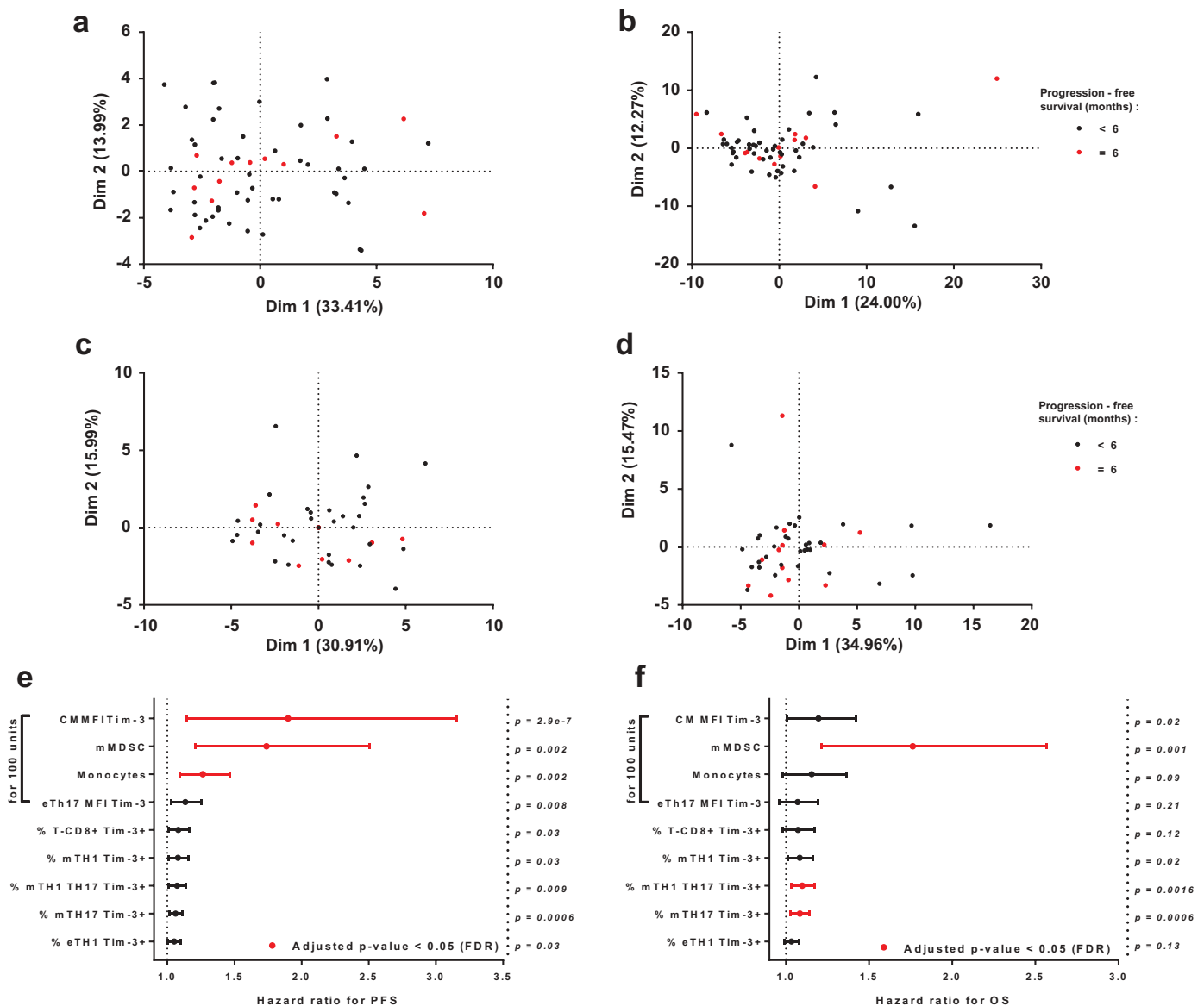


Figure 3. (a-b-c-d). Individual factor maps of four principal component analyses including: all myeloid parameters at day 0 (a); all lymphoid parameters at day 0 (b); all myeloid parameters at day 15 (c) and all lymphoid parameters at day 15 (d). Each individual is represented by a dot; red dots represent patients with progression-free survival greater than 6 months, and black dots represent patients with progression-free survival less than 6 months. Percentages given in brackets correspond to the percent of variance of initial data retained by the axis. (e-f). Forest plots of the hazard ratios and corresponding 95% confidence intervals estimated for variables significantly associated with progression-free survival (PFS) at day 15 from univariate Cox models (e). Forest plots for the same variables based on overall survival (OS) outcome (f). Significant variables after false-discovery rate (FDR) correction are displayed in red.

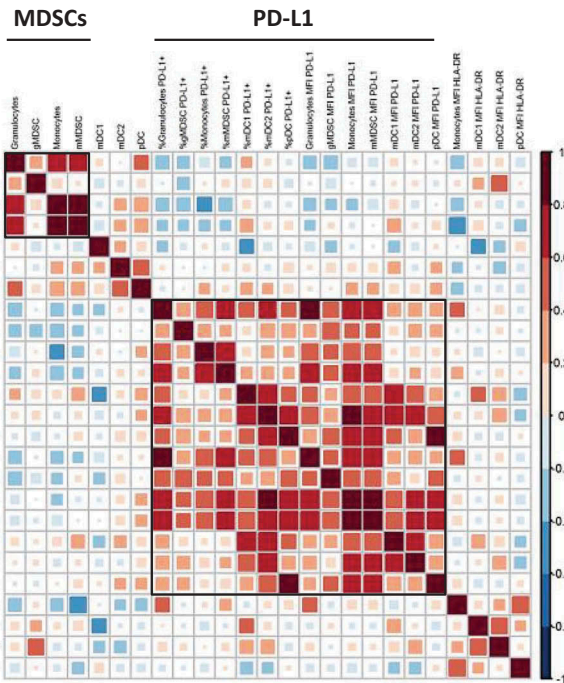
Results

T cell number and activation markers discriminate lung cancer patients from healthy volunteers

We first determined whether blood immune parameters could discriminate metastatic NSCLC from healthy volunteers. To do this we analyze 61 consecutive metastatic NSCLC patients before the introduction of nivolumab, as well as 12 sex- and age-matched healthy controls. We characterized the absolute number, frequency and mean fluorescence intensity (MFI) of various blood lymphoid and myeloid cells (Supplementary Figures 1–4 for gating strategy and Supplementary Table 1 for the list of immune subpopulations and markers). We analyzed 25 myeloid and 151 lymphoid variables, focusing on activation and differentiation markers.

The demographic and histopathologic characteristics of this cohort are described in Table 1. The median age was 66 years. The population was predominantly male (14 women (23%) and 47 men (77%)). Thirty-six patients (59%) had adenocarcinoma and 24 patients (39%) had squamous cell carcinoma. One patient (2%) had an undifferentiated carcinoma. Only six patients (10%) had never smoked. A total of 8 patients (13%) had locally advanced NSCLC and 53 (87%) had metastatic disease. Twelve patients presented partial response, 15 stable diseases and 34 progressive diseases at the CT-scan performed 2 months after initiation of therapy. Median progression-free survival (PFS) for all patients was 2.3 months (95% CI [1.8;3.9]). At the time of analysis, 13 patients (21%) had more than 6 months PFS. Median overall survival (OS) for all patients was 13.9 months (95% CI [11.9;22.9]).

a



b

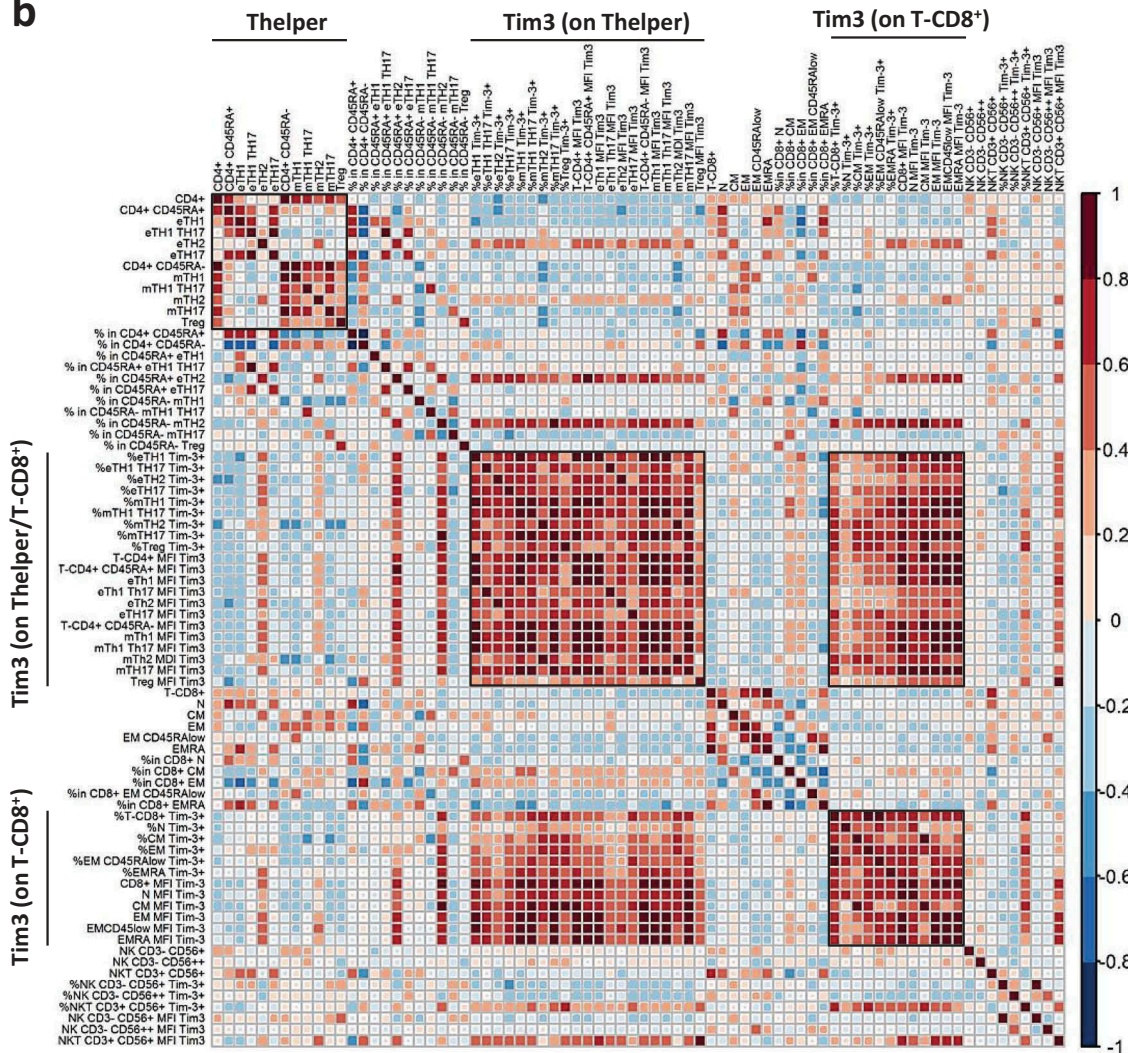


Figure 4. (a-b). Correlation matrices of myeloid parameters (a) and lymphoid parameters (b). Clusters of interest are displayed with black squares. Correlations were evaluated with Spearman's rank correlation coefficient.

We first performed a descriptive analysis of baseline immune parameters using two principal component analyses (PCA): one including all myeloid variables (Figure 1(a)) and the other including all lymphoid variables (Figure 1(b)). We observed that only lymphoid variables seem to have some variability that could separate cancer-bearing patients from healthy volunteers. Focusing on individual parameters for myeloid cells, we observed a significantly lower number of granulocytes (Wilcoxon rank-sum test $p = 0.01$) and a higher number of mMDSC (Wilcoxon rank-sum test $p = 0.01$) and mDC1 (Wilcoxon rank-sum test $p = 0.03$) in cancer patients compared to healthy volunteers (Figure 1(c)). A higher MFI value of HLA-DR activation markers on monocytes was observed in the cancer patient group (Wilcoxon rank-sum test $p = 0.005$) (Figure 1(d)) while proportions of myeloid cells expressing PD-L1⁺ did not differ between patients and healthy volunteers (Figure 1(e)).

Concerning lymphoid cells, we observed no significant changes in the number of major T cell subtypes (total CD4⁺ and CD8⁺ T cells), but a strong and significant decrease in NK cell numbers in cancer patients was observed (Wilcoxon rank-sum test $p = 0.004$) (Figure 1(f)). When we focused on the different subsets of CD4⁺ T cells, we did not observe a significant change in the proportions of total CD45RA⁺ or CD45RA⁻ cells (Figure 2(a)). While there was no variation in the proportions of the different CD45RA⁺ subpopulations, we observed a significant change of CD45RA⁻ subpopulation proportions due to a higher proportion of Th1 and a lower proportion of Th17 in the healthy volunteer group (permutation test $p = 0.048$) (Figure 2(b)). For CD8⁺ T cells, there was a decrease in central memory and naive CD8⁺ T cells in cancer patients (permutation test $p = 0.02$) (Figure 2(c)). Surprisingly, we observed significant changes for almost all lymphoid subpopulations in the proportions of Tim-3 and PD-1 expression. For each lymphoid population, we observed a decrease in the fraction of PD-1⁻ Tim-3⁺ for all subtypes in cancer patients and a decrease of double positive PD-1⁺ Tim-3⁺ for CD4⁺ T cells, CD8⁺ T cells and NK cells (Figure 2(d-f)).

Taken together, these data underline that lymphoid markers discriminate NSCLC patients from healthy volunteers, and suggest that cancer affects peripheral T cell response with an accumulation of Th17 and a decrease in antitumoral NK cells, Th1 cells and exhausted CD8⁺ T cells.

Association between baseline and early blood lymphoid and myeloid parameters, and outcome

To address the prognostic role of each biological baseline parameter, we first performed a descriptive analysis using two PCA: one including all myeloid variables (Figure 3(a)) and the other including all lymphoid variables (Figure 3(b)). We could not separate patients with clinical benefit from those without clinical benefit. To explore further, we performed univariate Cox analysis for each immunological variable, using variables as continuous data. For myeloid cells, only a high MFI PD-L1 on granulocytic MDSC value was significantly associated with poor PFS (log-rank test $p = 0.04$), and a high MFI PD-L1 on monocyte value was also associated with poor PFS but was borderline significant

(log-rank test $p = 0.053$). For lymphoid cells, only a high MFI PD-1 on effector memory CD8 was significantly associated with poor PFS (log-rank test $p = 0.04$). However, no variable remained significant after false discovery rate (FDR) correction (Supplementary Tables 2–3).

A similar analysis was also performed on variables tested 15 days after initiation of nivolumab treatment. Likewise, two PCA were performed: one including all myeloid variables (Figure 3(c)) and the other including all lymphoid variables (Figure 3(d)), which could not separate patients with clinical benefit from patients without clinical benefit. By univariate Cox analysis, only two myeloid markers and eight lymphoid markers were significantly associated with PFS. After FDR correction, only high monocyte and monocytic MDSC numbers, and high Tim-3 MFI expression in memory CD8⁺ T cells were significantly associated with poor prognosis (Figure 3(e)) (Supplementary Tables 4–5). Only mMDSC keep being significant after FDR correction on OS outcome (Figure 3(f)).

Correlations between variables taken at day 15 were tested. For the myeloid variables, we observed correlations between all PD-L1⁺ variables. mMDSC and monocyte were also correlated. For lymphoid markers, all variables associated with Tim-3 expression in lymphoid cells were correlated, apart from Tim-3 expression in NK cells (Figure 4(a and b)).

Together, these data underline that the baseline blood immune cell parameters considered here are unable to predict the outcome, but Tim-3 expression on lymphoid cells, number monocytes, and mMDSC after one injection of nivolumab are associated with outcome.

Day 15 immune variables reveal the importance of Tim-3 and mMDSC in primary and secondary resistance

To further explore the association between immune variables and survival, we fitted a predictive model of PFS using a boosting algorithm for the Cox model, on all variables tested at day 15, because these variables seemed more informative than day 0 variables when analyzed independently. This model was used to select variables, which are related to the outcome. The variables retained were: the number of effector Th1, Tim-3 MFI in effector Th1, Th17 and CM CD8⁺ T cells, the proportion of NK CD3⁻ CD56^{high}, the proportion of Tim-3⁺ effector Th1 and Th17 and CM CD8⁺ T cells, the number of monocytes and mMDSC. The algorithm generated a new composite biological variable which is a linear regression based on selected variables. Receiver Operating characteristic (ROC) curve was generated to determine the discriminative potential of the new variable to predict the outcome. We observe an AUC of 0.80 (specificity of 83% and sensitivity of 74%) which underline a good discriminative property (Figure 5(a)). This new variable was strongly associated with PFS and could discriminate patients with good and poor PFS (median PFS: Not reached (NR) *versus* 1.9 months; log-rank test $p < 0.0001$) (Figure 5(b)). Similar results were not obtained for OS (Figure 5(c)). The same model was also strongly predictive of PFS but not for OS when biological variables were analyzed at day 30, thus demonstrating the stability of the model at a different timepoint (median PFS of 1.8 months *versus* NR; log-rank test $p = 0.02$) (Figure 5(d-e)). Together, these data

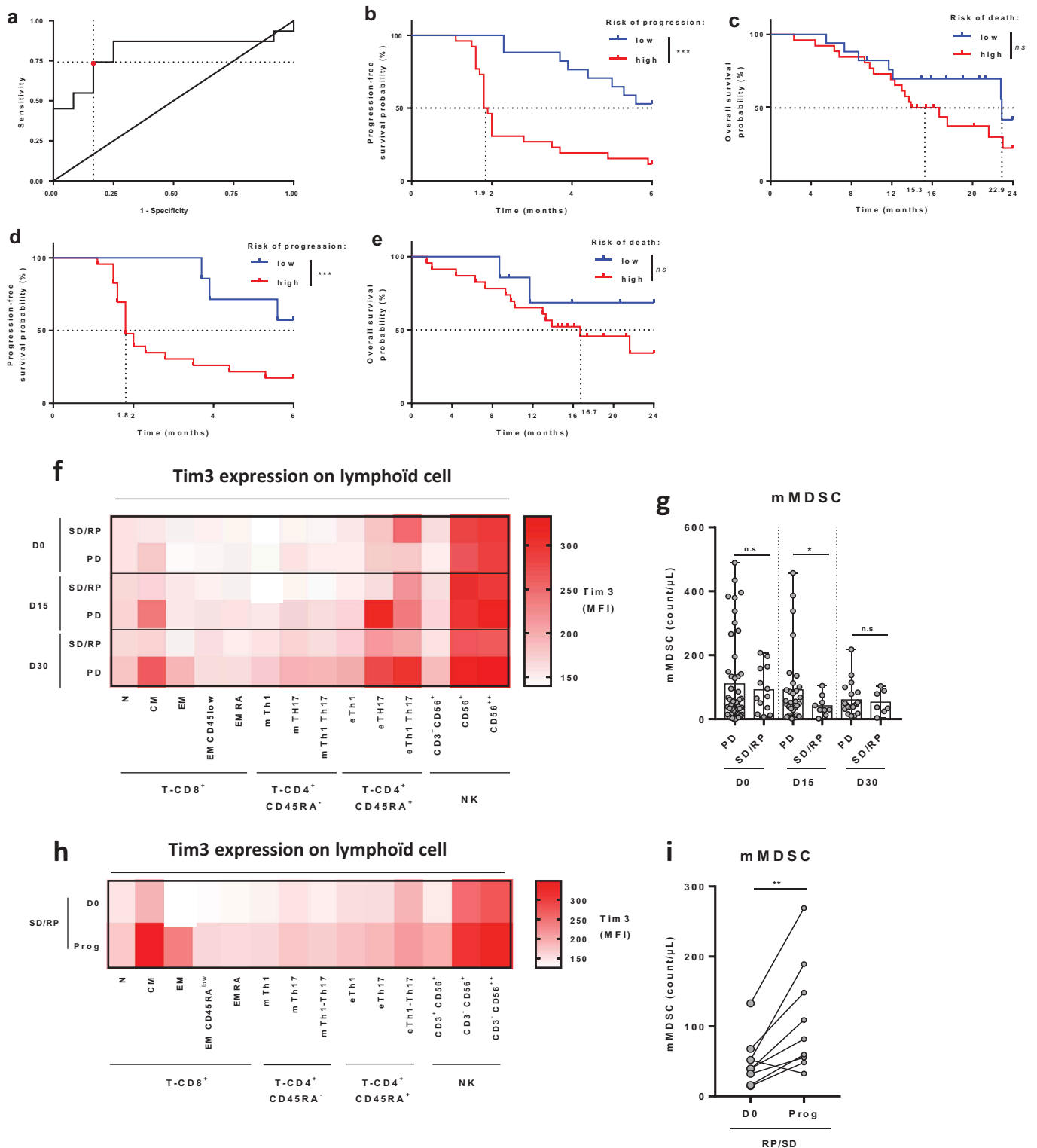


Figure 5. (a). ROC curve estimated using the linear predictor estimated from the Coxboost model adjusting for data at day 15. The chosen cutoff is represented by a red dot. (b-c). Kaplan-Meier estimates for progression-free survival (b) and overall survival (c); patients were stratified according to the value of the linear predictor estimated from the Coxboost model adjusted for data at day 15 on progression-free survival outcome: high risk (in red) or low risk (in blue). (d-e). Kaplan-Meier estimates for progression-free survival (D) and overall survival (E); patients were stratified according to the value of the linear predictor estimated from the Coxboost model for data at day 30 on progression-free survival outcome: high risk (in red) or low risk (in blue). (f). Representative heat map of Tim-3 median fluorescence intensity (MFI) on lymphoid cell subsets (CD8⁺ T, CD4⁺ T and NK subpopulations) at D0, D15 and D30 after anti-PD-1 introduction in responder/stable (PR/SD) versus progressive (PD) patients. (g). Scatter dot plot of mMDSC blood levels at D0, D15, and D30 after anti-PD-1 introduction in responder/stable (PR/SD) versus progressive (PD) patients. (h). Representative heat map of Tim-3 median fluorescence intensity (MFI) on lymphoid cell subsets (CD8⁺ T, CD4⁺ T, and NK subpopulations) at D0 and at the time of progression in initially responder/stable patients. (i). Scatter dot plot of mMDSC blood levels at D0 and at the time of progression in initially responder (RP)/stable (SD) patients.

*: $p < 0.05$; **: $p < 0.01$; ***: $p < 0.001$; ****: $p < 0.0001$; ns: not significant.

underline that early blood immune parameters detected after one injection of nivolumab are associated with outcome.

Univariate models and the CoxBoost model suggest that a high level of Tim-3 expression in peripheral lymphoid cells and an accumulation of mMDSC shortly after initiation of therapy are important factors that negatively affect the response to anti-PD-1 therapy. Indeed, during follow-up, we observed greater Tim-3 expression in progressive patients than in stable and responder patients in most of the lymphoid cell subsets after 1 or 2 injections of nivolumab (Figure 5(f)). When focusing on blood mMDSC numbers, we observed a rapid decrease in responders, while the number remained stable in non-responders (Figure 5(g)). We also obtained blood at progression for a small subset of patients ($n = 8$). As previously described, an increase in Tim-3 expression at progression in most lymphoid cell subpopulations (Figure 5(h)) and an increase in mMDSC blood levels (Figure 5(i)) was observed. These data suggest that high lymphoid Tim-3 expression and an accumulation of mMDSC are determinant factors in both primary and secondary resistance to nivolumab.

Galectin-9 expressing blood mMDSC impede Tim-3⁺ lymphoid cell functions and blunt efficacy of PD-1 blockade

To address the functional relevance of these observations, we collected blood from 10 metastatic NSCLC untreated with nivolumab. PBMC were isolated and restimulated with TCR triggering in the presence or not of nivolumab (Figure 6(a)). Interestingly, mMDSC expressed both PD-L1 and galectin-9, the respective ligands of PD-1 and Tim-3 (Figure 6(b)). In a context of PD-1 blockade, the capacity of PBMC to produce IFN γ was inversely correlated with the presence of mMDSC (Figure 6(c) left panel). When we focused our analysis on mMDSC phenotype, galectin-9, but not PD-L1, was negatively correlated with IFN γ secretion (Figure 6(c) center and right panel). In the absence of nivolumab, IFN γ -producing CD8⁺ T cells were inversely correlated with the presence of both PD-L1 and galectin-9 expressing MDSC (Figure 6(d)). Production of IFN γ by PBMC after nivolumab, *ex vivo* treatment was inversely correlated with the presence of Tim-3, but not PD-1 expressing CD8⁺ T cells (Figure 6(e-f)). In contrast, in the absence of nivolumab, the production of IFN γ by PBMC was inversely correlated with the presence of CD8⁺ T cells expressing both Tim-3 and PD-1 (Figure 6(g-h)). Otherwise, while nivolumab and anti-Tim-3 alone have only a modest and non-significant ability to restore IFN γ and TNF α secretion by PBMC of patients with NSCLC, the combination of the two antibodies strongly restores cytokine production (Figure 6(i)). Taken together, these findings underline that Tim-3 expression on CD8⁺ T cells and galectin-9 expression on monocytic MDSC blunt the secreting ability of CD8, and are involved in the mechanisms of resistance to nivolumab.

Discussion

Testing of peripheral blood markers is a non-invasive source of potential biomarkers in patients receiving

immune-checkpoint therapies. In this report, we propose that Tim-3 expression on blood circulating T cells, and accumulation of monocytic MDSC could be a surrogate early marker, for patients treated for NSCLC by nivolumab in second or further line therapy. In addition, these markers may also be used to detect secondary escape.

Few data exist addressing the prognostic role of blood immune cells in the setting of checkpoint inhibitor therapy. In the case of melanoma and ipilimumab studies, improved overall and progression-free survival were associated with baseline values, including low absolute neutrophil count, low neutrophil to lymphocyte ratio, low absolute monocyte count, low frequency of MDSC, high frequency of Treg, high frequency of lymphocytes and high eosinophil count,^{20,21} although such data are not currently validated in prospective studies. Dynamic changes during ipilimumab therapy in patients with melanoma including decreasing concentrations of Foxp3⁺ regulatory T cells, increasing absolute lymphocyte counts, and increasing eosinophil counts have also been associated with clinical benefit.^{22–24} Classical blood parameters could be associated with response to anti-PD-1. In a retrospective study including 607 patients with melanoma treated with pembrolizumab, elevated baseline eosinophil count and elevated lymphocyte count were both associated with improved overall survival¹¹. The role of immune parameters on avelumab (an anti-PD-L1 mAb) was recently addressed. In a phase I trial including 28 patients, 123 immune parameters were analyzed by flow cytometry prior to and following one, three, and nine cycles of avelumab. No statistically significant changes in any of the 123 immune cell subsets analyzed were observed at any dose level, or the number of doses of avelumab.²⁵ In a phase 1/2 study of nivolumab plus multi-peptide vaccine in patients with melanoma, an increased Treg frequency at week 12 was associated with progression and at baseline, antigen-specific CD8⁺ T cells were significantly lower in responders and stable patients compared with non-responders.²⁶ In a similar study testing the association of nivolumab with vaccine in melanoma, higher baseline Treg and MDSC populations were associated with poor response to therapy.²⁷ Recently, another study tested the role of blood parameters in 29 patients treated with pembrolizumab for melanoma. No parameter in baseline analysis was associated with response to therapy. In contrast, after the introduction of therapy, the authors observed a rapid activation of exhausted T cells. No blood parameter alone is a surrogate biomarker of response, but when combined with the assessment of tumor burden, a composite biomarker could predict patient survival under therapy.¹³

In our series, we addressed similar questions in the setting of NSCLC under nivolumab therapy. Like previous studies, no variable was significantly associated with PFS under anti-PD-1 at baseline. However, we highlighted an increase of mMDSC in patients at baseline like demonstrated by Yamauchi et al. in localized NSCLC with the same mMDSC gating strategy.²⁸ We observed that early accumulation of Tim-3 expressing lymphoid cells, and mMDSC were associated with resistance to nivolumab. Interestingly, in patients with initial response to nivolumab, we also observed accumulation of Tim-3

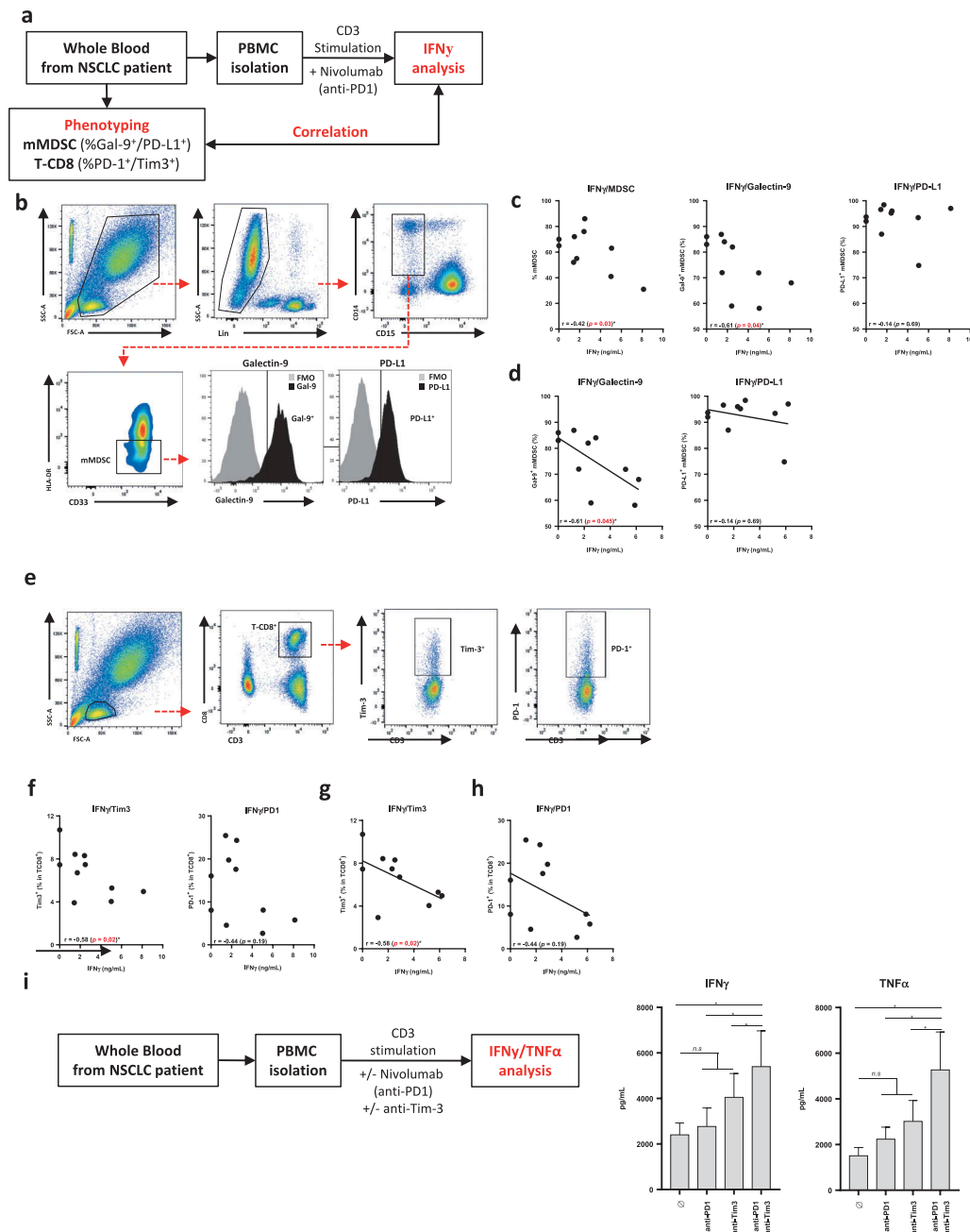


Figure 6. (a). Graphical representation of the strategy used to correlate PBMC immune profile (mMDSC and T CD8⁺ phenotype) with response to CD3 stimulation and PD-1 blockade *in vitro* (during 3 days). (b). Representative gating strategy used to analyze PD-L1 and galectin-9 expression on peripheral blood mMDSC in NSCLC patients ($n = 10$). FMO controls were used to identify PD-L1 and galectin-9 positivity. (c). Correlation curves of mMDSC level in PBMC (at day 0) (on the left), of the percentage of galectin-9⁺ mMDSC (in the middle) and PD-L1⁺ mMDSC (on the right) with IFN γ secretion level (after 3 days of CD3 stimulation and PD-1 blockade). Correlations were evaluated with Spearman's rank correlation coefficient. (d). Correlation curves of the percentage of galectin-9⁺ mMDSC (in the left) and PD-L1⁺ mMDSC (on the right) with IFN γ secretion level (after 3 days of CD3 stimulation but without PD-1 blockade). Correlations were evaluated with Spearman's rank correlation coefficient. (e). Representative gating strategy used to analyze PD-1 and Tim-3 expression on peripheral blood CD8⁺ T cells in NSCLC patients ($n = 10$). FMO controls were used to identify PD-1 and Tim-3 positivity (presented in SD2). (f). Correlation curves of the percentage of Tim-3⁺ T-CD8⁺ (on the left) and PD-1⁺ T-CD8⁺ (on the right) with IFN γ secretion level (after 3 days of CD3 stimulation and PD-1 blockade). Correlations were evaluated with Spearman's rank correlation coefficient. (g-h). Correlation curves of the percentage of Tim-3⁺ T-CD8⁺ (G) and PD-1⁺ T-CD8⁺ (H) with IFN γ secretion level (after 3 days of CD3 stimulation but without PD-1 blockade). Correlations were evaluated with Spearman's rank correlation coefficient. (i). Graphical representation of the strategy used to study anti-PD-1 and anti-Tim-3 blockade additive effects *in vitro* on NSCLC PBMC after CD3 stimulation (3 days) (on the left). IFN γ and TNF α secretions were analyzed by ELISA (on the right). *: $p < 0.05$; **: $p < 0.01$; ***: $p < 0.001$; ****: $p < 0.0001$; ns: not significant.

expressing lymphoid cells and mMDSC at secondary progression. Taken together, these data suggest that Tim-3 expression and monocytic MDSC accumulation are mechanisms involved in both primary and secondary resistance to anti-

PD-1 therapy. Previous reports suggest that secondary resistance to checkpoint inhibitors is associated with genetic mutation linked to the pressure of selection. Some reports suggest that neoantigen loss could occur through the elimination of

tumor subclones which are eliminating by activated T cells by anti-PD-1.²⁹ Some other reports describe mechanisms that involve loss-of-function mutations or LOH in genes including *HLA* genes, β 2-microglobulin, *PTEN*, *JAK1*, and *JAK2*, or the transporter for antigen presentation (*TAP1*) genes.³⁰ However, no report previously suggested Tim-3 or mMDSC as mechanisms of secondary resistance.

From a biological point of view, mMDSC expressed galectin-9, the ligand of Tim-3. Presence of Tim-3⁺ exhausted T cells and galectin-9 expressing mMDSC was associated with decreased CD8 secreting capacity. From a therapeutic point of view, we observed that anti-Tim-3 could restore *in vitro* the CD8 secreting property when combined with anti-PD-1, thus suggesting that Tim-3 expression is not only a biomarker of resistance but may also have a mechanistic role in this resistance. Previous reports in mice also suggest that depletion of MDSC using different strategies, enhance the efficacy of anti-PD-1 or anti-CTLA4 therapy.^{31–33} Together our data and previous mice experiments provide a strong rationale to combine mMDSC depletion and Tim-3 blockade in addition to anti-PD-1 therapy to fight against primary and secondary resistance.

In conclusion, our data propose that early induction of Tim-3 expression on lymphoid cells and mMDSC could be used to predict patient response to anti-PD-1 therapy in lung cancer. Moreover, Tim-3 blockade and mMDSC are involved in primary and secondary resistance to anti-PD-1 therapy. mMDSC and Tim-3 expression are associated with the reduced capacity of CD8⁺ T cells to produce IFN γ under anti-PD-1 therapy. These data strongly support the rationale for testing combination therapy of anti-PD-1 and anti-Tim-3 and/or MDSC depletion in these patients to improve the response rate to anti-PD-1/PDL1 therapy in lung cancer.

Abbreviations

anti PD-1	(Program death 1)
MDSC	myeloid derived suppressor cells
Tim3	T-cell immunoglobulin and mucin-domain containing-3

Authors' Contributions

Conception and design: E. Limagne, F. Ghiringhelli

Development of methodology: E. Limagne, C. Richard, M. Thibaudin, C. Truntzer

Acquisition of data (acquired and managed patients, provided facilities, etc.): E. Limagne, M. Thibaudin

Analysis and interpretation of data (e.g., statistical analysis, biostatistics, computational analysis): C. Richard, C. Truntzer

Writing, review, and/or revision of the manuscript: E. Limagne, C. Richard, M. Thibaudin, C. Truntzer, F. Ghiringhelli

Administrative, technical, or material support (i.e., reporting or organizing data, constructing databases and patients' recruitment): J.D. Fumet, A. Lagrange, L. Favier, B. Coudert

Study supervision: E. Limagne, F. Ghiringhelli

Disclosure of Potential Conflicts of Interest

No potential conflicts of interest were disclosed.

Competing financial interests

F. Ghiringhelli received honoraria for oral communication from Lilly, Sanofi, and Amgen and is an advisory board member for Merck Serano, Amgen, Sanofi. No other author has any potential conflict of interest to disclose.

References

- Torre LA, Bray F, Siegel RL, Ferlay J, Lortet-Tieulent J, Jemal A. Global cancer statistics, 2012. *CA Cancer J Clin*. 2015 Mar;65(2):87–108. doi:10.3322/caac.21294.
- Giroux Leprieur E, Dumenil C, Julie C, Giraud V, Dumoulin J, Labrune S, Chinet T. Immunotherapy revolutionises non-small-cell lung cancer therapy: results, perspectives and new challenges. *Eur J Cancer Oxf Engl* 1990. 2017;78:16–23.
- Califano R, Kerr K, Morgan RD, Lo Russo G, Garassino M, Morgillo F, Rossi A. Immune checkpoint blockade: a new era for non-small cell lung cancer. *Curr Oncol Rep*. 2016;18(9):59. doi:10.1007/s11912-016-0544-7.
- Borghaei H, Paz-Ares L, Horn L, Spigel DR, Steins M, Ready NE, Chow LQ, Vokes EE, Felip E, Holgado E, et al. Nivolumab versus docetaxel in advanced nonsquamous non-small-cell lung cancer. *N Engl J Med*. 2015 Oct 22;373(17):1627–1639. doi:10.1056/NEJMoa1507643.
- Herbst RS, Baas P, Kim D-W, Felip E, Pérez-Gracia JL, Han J-Y, Molina J, Kim JH, Arvis CD, Ahn MJ. Pembrolizumab versus docetaxel for previously treated, PD-L1-positive, advanced non-small-cell lung cancer (KEYNOTE-010): a randomised controlled trial. *Lancet Lond Engl*. 2016 Apr 9;387(10027):1540–1550. doi:10.1016/S0140-6736(15)01281-7.
- Diggs LP, Hsueh EC. Utility of PD-L1 immunohistochemistry assays for predicting PD-1/PD-L1 inhibitor response. *Biomark Res*. 2017;5:12. doi:10.1186/s40364-017-0093-8.
- Grigg C, Rizvi NA. PD-L1 biomarker testing for non-small cell lung cancer: truth or fiction? *J Immunother Cancer*. 2016;4:48. doi:10.1186/s40425-016-0153-x.
- Reck M, Rodríguez-Abreu D, Robinson AG, Hui R, Csösz T, Fülöp A, Gottfried M, Peled N, Tafreshi A, Cuffe S, et al. Pembrolizumab versus chemotherapy for PD-L1-positive non-small-cell lung cancer. *N Engl J Med*. 2016 10;375(19):1823–1833. doi:10.1056/NEJMoa1606774.
- Taube JM, Klein A, Brahmer JR, Xu H, Pan X, Kim JH, Chen L, Pardoll DM, Topalian SL, Anders RA. Association of PD-1, PD-L1 ligands, and other features of the tumor immune microenvironment with response to anti-PD-1 therapy. *Clin Cancer Res Off J Am Assoc Cancer Res*. 2014 Oct 1;20(19):5064–5074. doi:10.1158/1078-0432.CCR-13-3271.
- Garon EB, Rizvi NA, Hui R, Leighl N, Balmanoukian AS, Eder JP, Patnaik A, Aggarwal C, Gubens M, Horn L, et al. Pembrolizumab for the treatment of non-small-cell lung cancer. *N Engl J Med*. 2015 May 21;372(21):2018–2028. doi:10.1056/NEJMoa1501824.
- Weber R, Fleming V, Hu X, Nagibin V, Groth C, Altevogt P, Utikal J, Umansky V. Myeloid-derived suppressor cells hinder the anti-cancer activity of immune checkpoint inhibitors. *Front Immunol*. 2018;9:1310. doi:10.3389/fimmu.2018.01310.
- Weide B, Martens A, Hassel JC, Berking C, Postow MA, Bisschop K, Simeone E, Mangana J, Schilling B, Di Giacomo AM, et al. Baseline biomarkers for outcome of melanoma patients treated with pembrolizumab. *Clin Cancer Res Off J Am Assoc Cancer Res*. 2016 Nov 15;22(22):5487–5496. doi:10.1158/1078-0432.CCR-16-0127.
- Huang AC, Postow MA, Orlowski RJ, Mick R, Bengsch B, Manne S, Xu W, Harmon S, Giles JR, Wenz B, et al. T-cell invigoration to

- tumour burden ratio associated with anti-PD-1 response. *Nature*. 2017 04;545(7652):60–65. doi:10.1038/nature22079.
14. Rovati B, Mariucci S, Manzoni M, Bencardino K, Danova M. Flow cytometric detection of circulating dendritic cells in healthy subjects. *Eur J Histochem EJH*. 2008 Mar;52(1):45–52. doi:10.4081/1185.
 15. Legat A, Speiser DE, Pircher H, Zehn D, Fuertes Marraco SA. Inhibitory receptor expression depends more dominantly on differentiation and activation than “Exhaustion” of human CD8 T cells. *Front Immunol*. 2013;4:455. doi:10.3389/fimmu.2013.00455.
 16. Mahnke YD, Beddall MH, Roederer M. OMIP-017: human CD4 (+) helper T-cell subsets including follicular helper cells. *Cytom Part J Int Soc Anal Cytol*. 2013 May;83(5):439–440. doi:10.1002/cyto.a.22269.
 17. Cooper MA, Fehniger TA, Caligiuri MA. The biology of human natural killer-cell subsets. *Trends Immunol*. 2001 Nov;22(11):633–640. doi:10.1016/S1471-4906(01)02060-9.
 18. Roederer M, Nozzi JL, Nason MC. SPICE: exploration and analysis of post-cytometric complex multivariate datasets. *Cytom Part J Int Soc Anal Cytol*. 2011 Feb;79(2):167–174. doi:10.1002/cyto.a.21015.
 19. Binder H CoxBoost: cox models by likelihood based boosting for a single survival endpoint or competing risks [Internet]; 2013 [accessed 2018 Sep 21]. <https://CRAN.R-project.org/package=CoxBoost>.
 20. Ferrucci PF, Ascierto PA, Pigozzo J, Del Vecchio M, Maio M, Antonini Cappellini GC, Guidoboni M, Queirolo P, Savoia P, Mandalà M, et al. Baseline neutrophils and derived neutrophil-to-lymphocyte ratio: prognostic relevance in metastatic melanoma patients receiving ipilimumab. *Ann Oncol Off J Eur Soc Med Oncol*. 2016 Apr;27(4):732–738. doi:10.1093/annonc/mdw016.
 21. Martens A, Wistuba-Hamprecht K, Geukes Foppen M, Yuan J, Postow MA, Wong P, Romano E, Khammari A, Dreno B, Capone M, et al. Baseline peripheral blood biomarkers associated with clinical outcome of advanced melanoma patients treated with ipilimumab. *Clin Cancer Res Off J Am Assoc Cancer Res*. 2016 15;22(12):2908–2918. doi:10.1158/1078-0432.CCR-15-2412.
 22. Delyon J, Mateus C, Lefeuvre D, Lanoy E, Zitvogel L, Chaput N, Roy S, Eggermont AMM, Routier E, Robert C. Experience in daily practice with ipilimumab for the treatment of patients with metastatic melanoma: an early increase in lymphocyte and eosinophil counts is associated with improved survival. *Ann Oncol Off J Eur Soc Med Oncol*. 2013 Jun;24(6):1697–1703. doi:10.1093/annonc/mdt027.
 23. Ku GY, Yuan J, Page DB, Schroeder SEA, Panageas KS, Carvajal RD, Chapman PB, Schwartz GK, Allison JP, Wolchok JD. Single-institution experience with ipilimumab in advanced melanoma patients in the compassionate use setting: lymphocyte count after 2 doses correlates with survival. *Cancer*. 2010 Apr 1;116(7):1767–1775. doi:10.1002/cncr.v116:7.
 24. Simeone E, Gentilcore G, Giannarelli D, Grimaldi AM, Caracò C, Curvietto M, Esposito A, Paone M, Palla M, Cavalcanti E, et al. Immunological and biological changes during ipilimumab treatment and their potential correlation with clinical response and survival in patients with advanced melanoma. *Cancer Immunol Immunother CII*. 2014 Jul;63(7):675–683. doi:10.1007/s00262-014-1545-8.
 25. Donahue RN, Lepone LM, Grenga I, Jochems C, Fantini M, Madan RA, Heery CR, Gulley JL, Schlom J. Analyses of the peripheral immunome following multiple administrations of avelumab, a human IgG1 anti-PD-L1 monoclonal antibody. *J Immunother Cancer*. 2017;5:20. doi:10.1186/s40425-017-0220-y.
 26. Weber JS, Kudchadkar RR, Yu B, Gallenstein D, Horak CE, Inzunza HD, Zhao X, Martinez AJ, Wang W, Gibney G, et al. Safety, efficacy, and biomarkers of nivolumab with vaccine in ipilimumab-refractory or -naive melanoma. *J Clin Oncol Off J Am Soc Clin Oncol*. 2013 Dec 1;31(34):4311–4318. doi:10.1200/JCO.2013.51.4802.
 27. Gibney GT, Kudchadkar RR, DeConti RC, Thebeau MS, Czupryn MP, Tetteh L, Eysmans C, Richards A, Schell MJ, Fisher KJ, et al. Safety, correlative markers, and clinical results of adjuvant nivolumab in combination with vaccine in resected high-risk metastatic melanoma. *Clin Cancer Res Off J Am Assoc Cancer Res*. 2015 Feb 15;21(4):712–720. doi:10.1158/1078-0432.CCR-14-2468.
 28. Yamauchi Y, Safi S, Blattner C, Rathinasamy A, Umansky L, Juenger S, Warth A, Eichhorn M, Muley T, Herth FJF, et al. Circulating and tumor myeloid-derived suppressor cells in resectable non-small cell lung cancer. *Am J Respir Crit Care Med*. 2018 Sep 15;198(6):777–787. doi:10.1164/rccm.201708-1707OC.
 29. Anagnostou V, Smith KN, Forde PM, Niknafs N, Bhattacharya R, White J, Zhang T, Adleff V, Phallen J, Wali N, et al. Evolution of neoantigen landscape during immune checkpoint blockade in non-small cell lung cancer. *Cancer Discov*. 2017;7(3):264–276. doi:10.1158/2159-8290.CD-16-0828.
 30. Jenkins RW, Barbie DA, Flaherty KT. Mechanisms of resistance to immune checkpoint inhibitors. *Br J Cancer*. 2018 Jan;118(1):9–16. doi:10.1038/bjc.2017.434.
 31. Orillion A, Hashimoto A, Damayanti N, Shen L, Adelaiye-Ogala R, Arisa S, Chintala S, Ordentlich P, Kao C, Elzey B, et al. Entinostat neutralizes myeloid-derived suppressor cells and enhances the antitumor effect of PD-1 inhibition in murine models of lung and renal cell carcinoma. *Clin Cancer Res Off J Am Assoc Cancer Res*. 2017 01;23(17):5187–5201. doi:10.1158/1078-0432.CCR-17-0741.
 32. Kim SH, Li M, Trousil S, Zhang Y, Pasca Di Magliano M, Swanson KD, Zheng B. Phenformin inhibits myeloid-derived suppressor cells and enhances the anti-tumor activity of PD-1 blockade in melanoma. *J Invest Dermatol*. 2017 Aug;137(8):1740–1748. doi:10.1016/j.jid.2017.03.033.
 33. Holmgaard RB, Brachfeld A, Gasmi B, Jones DR, Mattar M, Doman T, Murphy M, Schaer D, Wolchok JD, Merghoub T. Timing of CSF-1/CSF-1R signaling blockade is critical to improving responses to CTLA-4 based immunotherapy. *Oncoimmunology*. 2016 Jul;5(7):e1151595. doi:10.1080/2162402X.2016.1151595.